01
2020 April
Volume 4 · Issue 1

MODERN ELECTRONIC TECHNOLOGY

SYNERGY
PUBLISHING PTE. LTD.

APSCI | creative commons | CNKI 中国知网 www.cnki.net 中国知识基础设施工程
Google scholar | Crossref | MyScienceWork

ISSN 2591-7110 01
9 772591 711207
Price: S$30.00

Volume 4 Issue 1 · April 2020 · ISSN 2591-7110 (print) ISSN 2591-7129 (online)

Modern Electronic Technology

Aims and Scope

Modern Electronic Technology (MET) is an open access, peer-reviewed scholarly journal which aims to publish original research articles, reviews and short communications that covers all area of electronic engineering technology. MET emphasizes on publishing high quality papers, as well as aims to provide a source of information and discussion platform for engineers, researchers, and electronic professionals worldwide.

Subject areas suitable for publication include, but are not limited to the following fields:

- Microelectronics
- Nanoelectronics
- Electronic Materials Technology
- Structure and Nature of Semiconductor
- Digital Technology
- Automation System

Publishing Cycle

Quarterly

Journal Homepage

http://ojs.s-p.sg/index.php/met

Key Features

- Open Access
- High Academic Level Editorial Board
- Easy and Fast Submissions
- Double Blind Peer Review
- Rapid Online Publication of Articles upon Acceptance
- Outlet for Academic Institutions and Industry

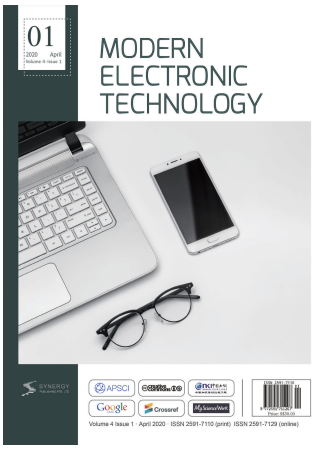

Volume 4 Issue 1 • April 2020
ISSN 2591-7110 (print) ISSN 2591-7129 (online)

Synergy Publishing Pte. Ltd.

E-Mail: contact@s-p.sg

Official Website: www.s-p.sg

Address: 12 Eu Tong Sen Street,
#07-169, Singapore (059819)

CONTENTS

Article

1 **Study on Cognitive Optical Network Structure and Self-optimization with the Application of Artificial Intelligence Technology**

Shengzhe Liang

6 **Simulated Curved Firing Electromagnetic Gun**

Jiuxin Gong Yuechang Shi Mingwei Xu

12 **Analysis of Drone Fleet Type and Quantity for Medical Package Distribution in Emergency System**

Yujie Jiang Shizhong Ma Shilong Zhu

16 **A Method for Measuring LC Resonance Frequency by Impulse Response**

Mingwei Xu Jiuxin Gong Yuechang Shi

Review

19 **Design and Implementation of Automatic Following Balancing Vehicle Based on UWB Positioning Principle**

Chenyu Zhang Fangyi Chen Zhongyun Kang

25 **Time Prediction Through A Congested Road Section**

Ziyi Cheng Ziqi Wei Xinhao Huang Ying Li

SYNERGY PUBLISHING PTE. LTD.

Modern Electronic Technology

https://ojs.s-p.sg/index.php/met

ARTICLE

Study on Cognitive Optical Network Structure and Self-optimization with the Application of Artificial Intelligence Technology

Shengzhe Liang*

Rutgers, The State University of New Jersey, New Brunswick, US

ARTICLE INFO

Article history
Received: 6 January 2020
Revised: 13 January 2020
Accepted: 9 April 2020
Published Online: 16 April 2020

Keywords:
Artificial intelligence technology
Cognitive optical network
Network structure
Self-optimization

ABSTRACT

Cognitive optical network is the intermediate to combine artificial intelligence technology with network, and also the important network technology to promote network intelligence level constantly. In the paper, it analyzes the cognitive optical network structure with the application of artificial intelligence technology by starting from the basic conditions of cognitive network and cognitive optional network on the basis of fully understanding the connotation of cognitive network and cognitive optical network, and explores its self-governance functions, so as to better realize the self-optimization and self-configuration of network.

1. Introduction

As the development level of information technology is promoted, internet traffic has shown a substantial increase over the years, reached to 2ZB in 2019, and increased the standard of network bandwidth demands. Since traditional network transmission technologies cannot meet the network operating demands, it is certain that new network transmission technologies will be generated as the replacement. Therefore, optical link coding technologies, super-channel technologies, and optical modulation technologies have been practiced in network transmission at different levels over the years. These new technologies are mainly deployed in the original optical network, and can largely increase the complicity of network environment. Meanwhile, the same optical fiber will exert direct influence on network transmission quality and transmission speed after being shared by different systems due to the increase in transmission capacity and the requirements of transmission speed. However, optical network is an autonomous network that is easy to maintain and manage, with low manual intervention demand, and can meet the demand of the current network transmission for intelligent management. On this basis, cognitive optical network has emerged in recent years. It combines network characteristics with artificial intelligence technology advantages, and is equipped with self-governance function. It is of great significance to improve network transmission quality and service quality by exploring how to solve the aforementioned problems with artificial intelligence technology and realize self-optimization.

**Corresponding Author:*
Shengzhe Liang,
Male, a student majored in Computer,
The State University of New Jersey, 57 US Highway 1,New Brunswick, NJ 08901-8554;
E-mail: shengzhe.liang@rutgers.edu.

 DOI: https://doi.org/10.26549/met.v4i1.3100

2. Cognitive Network and Cognitive Optical Network

2.1 Overview to Cognitive Network

Cognitive network can not only detect network environment, but also make intelligent plan for network by making full use of the local automatic network environment adaptability, and constant learning capacity. Besides, it can also make correct decisions to realize end-to-end objectives, and then lay a good development foundation for the follow-up dynamic changes and dynamic adjustment of network. Cognitive network is equipped with cognitive functions and learning functions. The most basic action to carry out cognitive network will form a complete cognition cycle, which includes five modules, i.e., Observe, Plan, Act, Orient, and Decide. In respect of Observe, it mainly adopts monitoring equipment in the real-time observation of network environment and network state, summarize the acquired data and provide basis for the Plan, while using the learning module to store the acquired data. In the process of Orient, suitable action mode should be selected by combing with the actual conditions about the background of observed information. After entering the phase of Decide, the cognitive network will formulate end-to-end system objective based on the actual act model selected and the plan achievements, and confirm suitable act in the end [1]. Finally, the link of Act is to ensure the execution of final decision in the network. Specific cycle process is as shown in Figure 1. This cycle can process new events in the network by constant cycle, and based on this characteristic, cognitive network is also called as autonomous network, and can optimize and configure as per network environment and network dynamics, and realize self-healing.

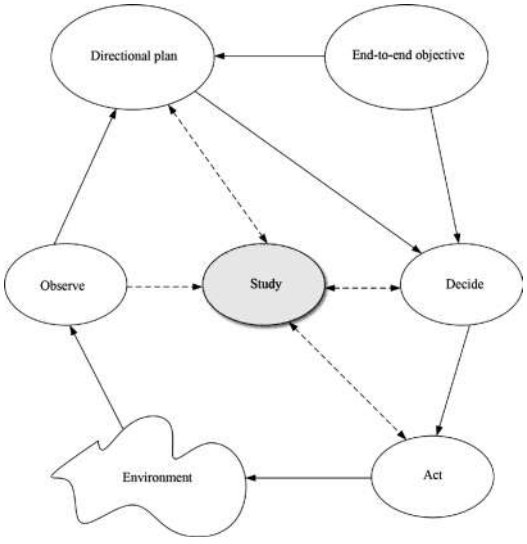

Figure 1. Schematic Diagram of Cognitive Network Cycle

2.2 Overview to the Cognitive Optical Network

Cognitive optical network has been the new direction of network technology studies over the years. Cognitive Heterogeneous Reconfigurable Optical Network Project (CHRON) funded by the European Union is currently the most successful research achievement at home and abroad, and its main objective is to develop cognitive optical network, provide support to control and manage the next generation of heterogeneous and optical network, and then become one of the major support technologies for the future development of internet. Cognitive Heterogeneous Reconfigurable Optical Network Research Project has completed the experimental research, and built intensive network architecture based on the research objective. Specific structure conditions are as shown in Figure 2. As can be seen from the figure, the project research is based on the deformation of distributed and intensive structures, but it is focused on the application of intensive type in test platforms [2]. As the most important part of the structure, cognitive decision system (CDS) exerts the effect of network event processing and the required management of network transmission, while network element is the key to ensure that cognitive actions can take effect in network operation. It is requested to consider the real-time status of network operation in structure architecture, and make full use of the previous knowledge to optimize network performance.

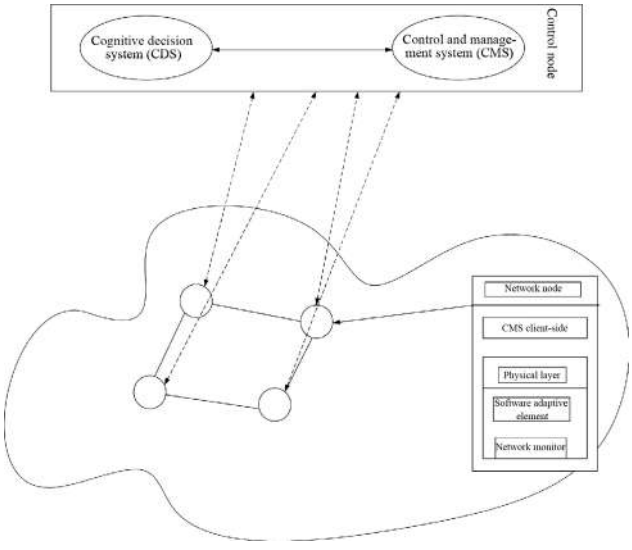

Figure 2. Cognitive Optical Network Structure Chart

Cognitive decision system (CDS) mainly exerts the effect of collecting monitoring information in network and sending management and control decisions to all cognitive decision systems (CDS) based on the control system and management system, while the self-optimization and

DOI: https://doi.org/10.26549/met.v4i1.3100

self-configuration of cognitive optical network are realized by extensively collecting network dynamic operating conditions via cognitive decision system, sending decisions to cognitive decision system (CDS), and activating self-adaptive elements.

3. Key Technologies and Structure of Cognitive Optical Network with the Application of Artificial Intelligence Technology

The compositions and structures of cognitive optical network mainly include five aspects, i.e., intelligent monitoring system, cognitive decision system, cognitive control system, cognitive study, the dynamic adjustment of structure and automatic configuration respectively. Although each system has different functions and different divisions of labor in the cognitive process, all parts are closely connected, and will affect the function of the cognitive optical network, in case of any missing parts. Specifically speaking, the structural conditions and key technical analysis of all parts are as shown below:

3.1 Intelligent Monitoring System

The main function of intelligent monitoring system is network environment monitoring, and is equivalent to the observation mentioned above. Advanced optical performance monitoring technologies are used in monitoring, in respect of the physical layer. Such technology is equipped with digital signal processing function, and can provide the required feedback signal to the monitoring system, and then give comprehensive feedbacks about network damage conditions or signal defects, so that the cognitive optical network can recognize fast and make plans, realize autonomous optimization and configuration, and rebuild network operating environment[3]. In order to meet the demand of network users and the requirements put forward for service quality, a core module is set in the intelligent monitoring system—optical signal performance detection module, which can transmit the acquired information contents to network management and network decision system, and then express that the system has received information parameters provided by electric fish of the optical field in combination with the optical communication system and its corresponding receiver. Besides, channel distortion also regards data model as the supplementary algorithm of the electric field, to acquire real-time monitoring on the link damage information, and finally complete the automatic compensation of the electric field, and all the confirmed linear optical channel parameters, including polarization mode dispersion and dispersion, etc. are within the scope of isostatic compensation. Besides, intelligent monitoring system can also monitor transmission parameters, such as the polarization rotation parameters.

3.2 Cognitive Decision System

As the most important part of cognitive optical network, cognitive decision system works as the brain of cognitive optical network, to make decisions, transmit to the control and management links, etc., and then realize the self-optimization and self-configuration of cognitive optical network. In system operation, it will simultaneously analyze the monitoring information and the knowledge base, and put the currently acquired observation information in previous knowledge experience for specific analysis, and then carry out comprehensive analysis and judgment based on the occurred events and current conditions, and formulate the best processing schedule, so as to realize the end-to-end objective effectively [4]. In the operation process of cognitive optical network, service and flow demand is the most basic supply of cognitive decision system. The cognitive optical network can seek for similar previous scenes and the decisions made thereby in the knowledge base based on the current network operating conditions during the operation, and then judge and make decisions based on the current operating conditions, store the analysis in the learning module, and improve learning capacity. Besides, it can also directly influence the future action of cognitive decision system, and then realize the end-to-end objective by network element adjustment based on the control and management system, and always realize the optimization of network transmission.

As can be seen from the operation and effect of cognitive decision system, it is closely related to network monitoring system and control system, and can form completed cognition cycle with two systems, while exerting its effect. Meanwhile, the cognitive optical network also has a specific knowledge base, which can search for information generated in all cognitive processes. It is generally arranged in the learning module, and will be updated in real time [5]. Therefore, a general database and specific database have also been formed in the cognitive optical network, and these two items can be activated and then implement information retrieval simultaneously in the cognitive process. The cognitive decision system can make decisions based on the current network operating conditions, and send instructions to network elements via the control system, and then network elements will complete decisions made by the cognitive decision system as the basic executing unit. In

 DOI: https://doi.org/10.26549/met.v4i1.3100

order to prevent network transmission quality from being influenced in the process, different routes can be used when setting new channels.

3.3 Cognitive Control System

Cognitive optical network mainly adopts distributed type as the main mode of management and control, but private or independent agreement contents will be increased in the construction of control system due to the difference in technologies, equipment and manufacturers, and such condition will largely increase the difficulty of network control, and influence the utilization efficiency of network resources. Therefore, the difference in the transmission quality and service quality incurred by the difference in transmission technologies and service demands should be considered in the development of cognitive optical network, to build a highly heterogeneous network operating environment [6]. There are domestic and foreign practices in this direction, such as GMPLS protocol family ASON (Automatically Switched Optical Network), GMPLS/PCE network control panel and SDN/Openflow SDON (Software Defined Optical Network), which have taken these heterogeneous conditions into considerations, optimized and adjusted the optical network structure accordingly, and then ensured that the control panel can be self-optimized based on actual network conditions, while executing the decisions made by the cognitive decision system.

3.4 Cognitive Study Structure

The intelligent characteristics of cognitive optical network can be mainly reflected by cognitive study, which will take effect in the operation of intelligent monitoring system. The study can be specific to network operation standard requirements, cognitive process plan, cognitive decisions and other series of process, and can ensure the real-time updating of knowledge base, apply the learned contents to handle network events in real time, and complete the target task of cognitive decision system. Cognitive study is mainly supported by machine study, and the common method is intelligent algorithm. Machine study is also called as case-based reasoning, which will associate with similar previous scenes and experience by reasoning the acquired knowledge experience, while solving new problems, and then adjusting parameters based on changes of the condition, and as processed events are increased, cases in the knowledge base will also increase constantly, so richer experience can be acquired while handling network events, and then it will improve the capacity of the system to solve problems[7]. Meanwhile, the system can also predict the future development conditions of network transmission by summarizing previous experience, so as to make predictable decisions and decrease the direct influence incurred by network transmission.

3.5 Dynamic Adjustment and Automatic Configuration of Structure

Cognitive optical network emphasizes on realizing end-to-end objective, and should always regard the objective as the center to adjust parameters and configurations in the cognitive process and the decision execution process, and ensure that construction characteristics of physical layer and parameters of the network layer can meet all end-to-end objective requirements at all times[8]. Dynamic adjustment of structure and automatic configuration is the main approach to realize the function, and can carry out operations by software programming or software self-customization module.

4. Conclusion

To sum up, cognitive optical network is of important value and significance to the development of network intelligence as the new topic and new direction of research on network technology over the years, but current researches are still in the initial phase, and lack of experience in sorting out the structure of cognitive optical network and the corresponding design. We should cognize the connotation, function and structure of cognitive optical network correctly, understand its composition structure, define the specific reflection of intelligence based on the analysis, so that we can focus on the intelligent function and intelligent service of cognitive optical network in future development, perfect technical system, and then provide a solid guarantee for the improvement of network service quality and the transmission quality level. This paper still has deficiencies in simple analysis, and merely discusses how to realize the self-optimization of cognitive optical network and its specific structure. It is hoped that we can summarize research achievements constantly in future research, deepen research contents, and improve research depth and width.

References

[1] Huang Haiqing, and Li Weimin. Research on Cognitive Optical Network Structure Based on Artificial Intelligence Technology [J]. Optical Communication Technology, 2016, 40(5):15-18.

[2] Fu Dong. Research on the Perceptive Transmission Technology of Cognitive Optical Network [D]. Sich-

DOI: https://doi.org/10.26549/met.v4i1.3100

uan: University of Electronic Science and Technology of China, 2019.
[3] University of Electronic Science and Technology of China. A Master-slave Signal Transmission Method in Cognitive Optical Network: CN201710959557.1 [P].2018-01-23.
[4] Ruan Xiaogang, Pang Tao, and Yu Jianjun. Phototaxis Control of Robot Based on the Neural Network Cognitive Mechanism of Boltzmann Machine [J]. Control and Decision-making, 2014, (12):2189-2194.
[5] Shenyang Aerospace University. A Deep Belief Network Intelligence Extraction Device in Cognitive Information Confrontation: CN201821413847.2 [P].2019-04-23.
[6] Wang Qian. "The Light of Reason" and "Experience Network"—Comparison of Two Cognitive Modes [J]. Journal of Dialectics of Nature, 2018, 40(12):94-100.
[7] Wei Jie. A Holographic 3D Interactive Display System Based on Artificial Intelligence Visual Recognition Technology: CN201720957226.X [P].2018-01-30.
[8] Editorial Department of the Journal (Summary), Zhang Chenglong (Planner/Executer). Cognitive Artificial Intelligence [J]. Entrepreneur Information, 2018, 000(007):P.15-28.

 DOI: https://doi.org/10.26549/met.v4i1.3100

SYNERGY PUBLISHING PTE. LTD.

Modern Electronic Technology

https://ojs.s-p.sg/index.php/met

ARTICLE

Simulated Curved Firing Electromagnetic Gun

Jiuxin Gong* **Yuechang Shi** **Mingwei Xu**

School of Information Engineering, North China University of Science and Technology, Tangshan, Hebei, 063210, China

ARTICLE INFO

Article history
Received: 17 January 2020
Revised: 24 January 2020
Accepted: 9 April 2020
Published Online: 16 April 2020

Keywords:
Electromagnetic cannon
OpenMV4
STM32F407
Servo head
Laser radar.

ABSTRACT

The device uses a self-made electromagnetic cannon and a control charging and discharging circuit to constitute the launching device of the electromagnetic cannon. The two-degree-of-freedom control PTZ controls the angle and direction of the electromagnetic cannon. It uses dual power supplies to power the main control board and electromagnetic cannon device. The microprocessor STM32F407 is used as the control core of the electromagnetic cannon, and the TCA8418 IIC matrix keyboard is used to adjust the distance and angle. The OpenMV4 automatically searches for the guide mark and captures the image shape and color blocks in real time to control the electromagnetic cannon to hit the round bullseye. . In addition, it also uses Lidar to measure the distance between the calibration point and the ring target, and uses OpenMV4 to realize the automatic search and launch of the electromagnetic cannon.

1. System Solutions

This system is mainly composed of five parts, including a main control module, an electromagnetic emission device, a camera recognition module, a power module, and a PTZ. The following is the design and demonstration process of the system scheme.

1.1 Technical Route

The system uses STM32F407 as the control system, and the switching power supply with wide voltage input and wide voltage output is used as the power supply system to control the output voltage. The design is to realize: the barrel is adjustable in the horizontal and vertical elevation directions, and the projectile is ejected with electromagnetic force to hit the target ring target. At the same time, the relevant parameters are displayed on the LCD display.

The general block diagram of the system is shown in the figure:

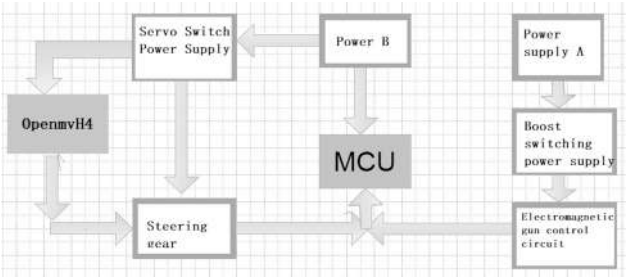

Figure 1. general block diagram of the system

**Corresponding Author:*
Jiuxin Gong,
School of Information Engineering, North China University of Science and Technology, Tangshan, Hebei, 063210, China;
E-mail: 930525332@qq.com.

DOI: https://doi.org/10.26549/met.v4i1.3242

1.2 Mechanical Solution

The gimbal is used as the base, the electromagnetic cannon is used as the launching device, and the OPENMV camera is used to lock the guide mark. At the same time, the main control board and the electromagnetic gun control device are placed on the bottom plate.

1.3 Hardware solution

The hardware consists of the main control microcontroller STM32F407, OPENMV H4 camera, Lidar, switching power supply module, and matrix keyboard.

1.3.1 Master

STM32MCU is fast, small, stable, rich in resources, and affordable.

Option 1: Use STMicroelectronics' STM32 F1 microcontroller.

The STM32 F1 microcontroller clock frequency reaches 72MHz, which is the highest performance product in its class; the basic clock frequency is 36MHz. As a development board for beginners, the STM32F103 can meet most of our functional needs.

Option 2: Use STMicroelectronics' STM32 F4 microcontroller.

The highest operating frequency of STM32F4 is 168Mhz, while STM32F1 is 72Mhz; STM32F4 has ART adaptive real-time accelerator, STM32F1 requires waiting period; STM32F4's FSMC uses a 32-bit multiple AHB bus matrix, which significantly improves the access speed compared to STM32F1 bus.

Finally, from the perspective of the proficiency of the chip and the clock frequency, it was decided to use the STM32F407 microcontroller in the second scheme.

1.3.2 Camera

Option 1: Use OPENMV4

OpenMV camera is a compact, low power, low cost circuit board that can easily complete machine vision applications. Via high-level Python scripts instead of C / C ++.

Option 2: Digital camera MT9V032

The driving configuration chip is integrated in the drill wind camera, and the dynamic threshold can be binarized with the automatic exposure function.

The title requires the ability to automatically search for a target and bombard a red ring target. In contrast, the 0penMV camera can recognize color images, so choose option one.

(1) Power supply

Option 1: Switching Power Supply RY3834

The advantages are small size, light weight, high efficiency (generally 60 ~ 70%, while linear power supply is only 30 ~ 40%), strong self-interference resistance, wide output voltage range, modularity.

The main disadvantage is that the DC voltage obtained after rectification usually causes a voltage change of 20% to 40%.

Option 2: Linear voltage regulator LM2596

The LM2596 is a switching voltage regulator for a step-down power management monolithic integrated circuit, capable of outputting a 3A drive current, and has good linearity and load regulation characteristics.

Considering the small size and high efficiency of the switching power supply, the first option is selected.

(2) Steering gear

Option 1: Futaba s3010 servo

The S3010 steering gear is a full resin gear, suitable for use in primary electric / oil-powered car models, electric / oil-powered ship models, general fixed-wing and small fixed-wing models, and medium-level oil-powered / electric 30-level helicopters.

Option 2: DG 995 steering gear

Digital servos have fast response, accurate angles, high torque, double bearings, small internal resistance, non-shake rudder, stall protection function, completely get rid of the phenomenon of servo shake, stalled burnout and other phenomena.

During the debugging process, the Futaba s3010 servo was selected to find the guide mark, and the gun barrel wobbled, resulting in angular deviation. Therefore, the DG 995 digital servo with debounce function was selected in the second scheme to improve the stability.

(3) keyboard

Option 1: TCA8418 matrix keyboard

The TCA8418 is a keyboard scan device with integrated ESD protection. It has 18 GPIOs, which can support up to 80 keys through the I2C interface.

Option 2: Traditional buttons

The independent button type is a single button circuit composed of I / O port lines directly. The advantage is that the work of each button will not affect the state of other I / O port lines. Although the programming is simple, the single-chip IO port is seriously wasted, and the IO resources of the single-chip microcomputer system are limited.

The TCA8418 matrix keyboard has strong operability, short debounce time, and convenient use. Considering Option 1 comprehensively.

2. Theoretical Analysis

2.1 Analysis of Electromagnetic Gun Model

The coil electromagnetic gun is mainly composed of a

 DOI: https://doi.org/10.26549/met.v4i1.3242

barrel, an excitation energy source, a relay, and a barrel. A single-stage or multi-stage excitation coil is closely wound on the barrel, and the excitation energy is a large-capacity capacitor. Based on the principle of electromagnetic induction, the control triggers a control switch to discharge, so that the discharge circuit is turned on, and a large instantaneous pulse of current passes through the coil, which generates a magnetic field. The transient magnetic field generated by the exciting coil causes the coil or ferromagnetic projectile to generate an induced current or magnetization, and then forms a magnetic force that attracts each other, thereby driving the coil or ferromagnetic projectile to move.

2.2 Coil Body Stress

The elastic body a is wound with a certain number of coils, as shown in Figure 2. When the solenoid passes a current i, the induced current of the elastic body coil is i. For the convenience of calculation, at the moment of interaction, it can be considered as constant. According to Ampere force and Stokes formula;

$$d\vec{F} = i_2 dl * \vec{B} \tag{1}$$

$$\oint \vec{B} \circ d\vec{l} = \iint_S (\nabla * \vec{B}) \circ d\vec{S} \tag{2}$$

$$\vec{F} = \oint_l i_2 d\vec{l} * \vec{B} = i_2 \nabla \varphi \tag{3}$$

The formula for the translational force of the coil in the magnetic field can be deduced. The translational force at the center of the coil is zero, and the translational thrust at the bottom of the coil is the largest. Therefore, the cannonball is placed at the bottom when it is launched.

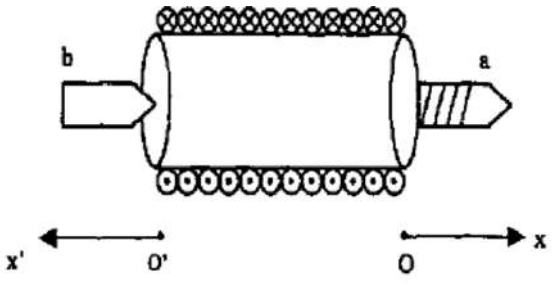

Figure 2. Force analysis

2.3 Ballistic Kinematics Analysis

According to Newton's second law, the differential equation of kinematics of the parabola can be obtained as:

$$m\frac{dx^2}{dt^2} = -\frac{1}{2}i^2\frac{dl_x}{dt} \tag{4}$$

2.4 Energy Calculation

Set the ferromagnetic projectile outside the solenoid port, the distance is x-l/2 (Initial position of the projectile), If x-l/2 Much smaller than the solenoid length l, Then the magnetic field strength at the projectile can be approximated as

$$H = \frac{l}{|x| + \frac{l}{2}}ni \tag{5}$$

Magnetic flux through the cross section of the projectile:

$$\varphi_m = \frac{l}{|x| + \frac{l}{2}}\mu_0 niS \tag{6}$$

According to the continuous flux theorem and the definition of inductance, the inductance of the solenoid is:

$$L_x = \frac{nl\varphi_M}{i} \tag{7}$$

The total system energy is:

$$W_m = \int_0^{\phi_m} id\phi_m = \frac{1}{2}L_x i^2 \tag{8}$$

3. Theoretical Parameters

3.1 Relationship between Emission Distance and PWM

Use the transmission distance as the independent variable and the PWM value as the dependent variable to explore the relationship. However, the magnitude of the supply voltage affects the transmission distance, so first determine the optimum value of the supply voltage.

① When the power supply voltage is 21.81V

Table 1. Distance and PWM value

Distance mean	PWM value
200	4050
210	4100
223.5	4130
252	4200
277.5	4500

The function fit is shown in the figure:

DOI: https://doi.org/10.26549/met.v4i1.3242

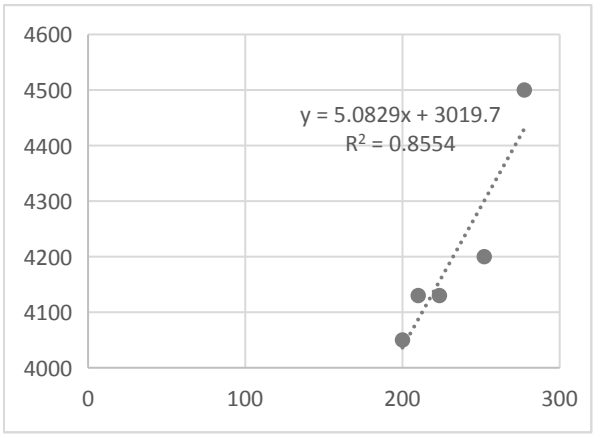

Figure 3. Relation between transmission distance and PWM

The resulting functional relationship is:

$$Y = 5.0829X^2 + 3019.7 \quad (9)$$

② When the power supply voltage is 24.84V

Table 2 Distance and PWM values

Distance mean	PWM value
225	3360
250	3300
266	3260
273	3200
296.5	3140

The function fit is shown in the figure:

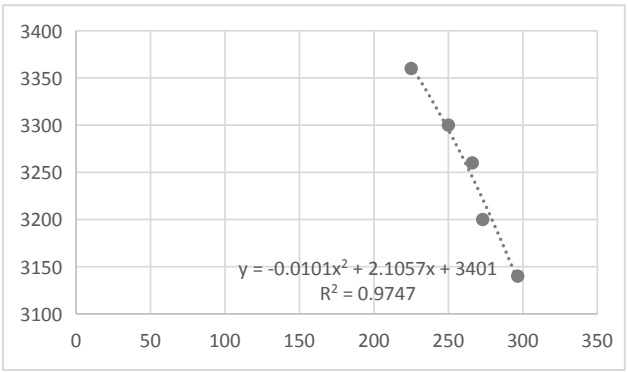

Figure 4. The relationship between the transmission distance and the PWM

The resulting functional relationship is:

$$Y = -0.0101X^2 + 2.1057X + 3401 \quad (10)$$

The experiment found that when the power supply voltage was 24.84V, the fitted degree of the function sought was the best and the deviation was the smallest.

3.2 Relationship between Angle and PWM

The title requires that the circular target is placed horizontally on the ground, and the position of the bull's eye is within the range of an angle±30 degree from the center axis. For the convenience of calculation, 30 ° left of the central axis is used as the experimental calibration 0 °, and 30 ° right of the central axis is used as the experimental calibration 60 °. The following is the recorded experimental data:

Table 3. Angle and PWM values

Angle (X)	PWM value (Y)
0	3100
10	2950
30	2680
50	2420

The function fit is shown in the figure:

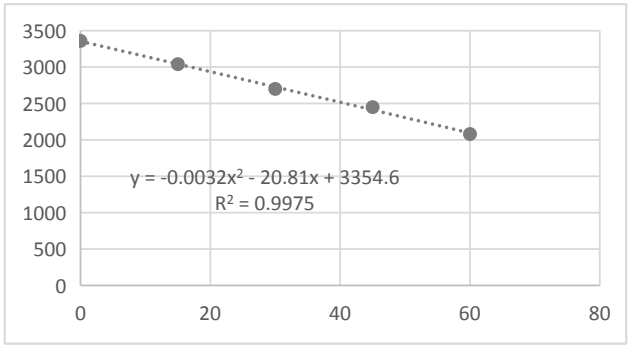

Figure 5. Relationship between angle and PWM

The resulting functional relationship is:

$$Y = -0.0032X^2 - 20.81X + 3354.6 \quad (11)$$

4. Circuit and Programming

4.1 Design of the Circuit

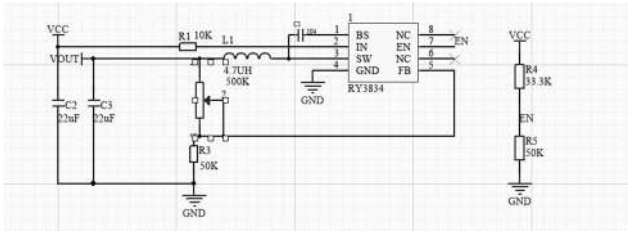

4.2 Control Scheme

Using PID control algorithm
Option 1: Position-type PID control.

Positional PID is the actual position of the current system, the deviation from the expected position you want to achieve, PID control. When the position type PID reaches saturation, the error will still continue to accumulate under the action of integration. Once the error starts to change in reverse, the system needs a certain time to exit from the saturation region, so when u (k) reaches the maximum and minimum, it must stop Integral effect, and there must be integral limit and output limit.

So when using positional PID, we generally use PD control directly.

Option 2: Incremental PID control.

Incremental PID is to increment the position-type PID. At this time, the controller outputs the difference between the position values calculated at two adjacent sampling times, and the result is an increment, that is, the value of the last control amount. On the basis, the amount of control needs to be increased (negative value means decreased).

Accumulation is not required in incremental PID. The determination of the control increment Δu (k) is only related to the last 3 sampling values. It is easy to obtain a better control effect through weighting processing, and the incremental operation will not seriously affect the work of the system when a problem occurs in the system. To sum up, choose the second incremental PID.

4.3 Program Design

(1) Program Function Description

The high and low level of the Io port of the single-chip microcomputer is controlled by the program, thereby controlling the opening and closing of the relay to realize the charging and discharging of the capacitor, thereby generating an instantaneous voltage change, and the changed voltage generates a magnetic field to drive the small iron rod to be driven outward by the electromagnetic force.

(2) Partial Program Explanation Display Part

By controlling the FSMC LCD to realize the mode, angle and distance display, it is more intuitive to see the change of variables. Keyboard part: TCA8418 matrix keyboard adopts analog IIC communication, and uses a minimum number of IO ports to control more keys, which greatly saves the resources of the microcontroller. Laser ranging: The target distance is transmitted to the single-chip microcomputer by serial communication.

5. System Test Results

5.1 Xperimental Design

Design the circuit diagram. Use an enameled wire with a diameter of 1.2mm to wind on a plastic straw with an inner diameter of about 1cm and a length of 18cm. The enameled wire is a 5cm long solenoid. It is powered by 24V DC, and a 5V DC relay is used to control the charge and discharge of an electrolytic capacitor. The bullet body is an ordinary nail head. Put the projectile into the bottom of the solenoid during the experiment.

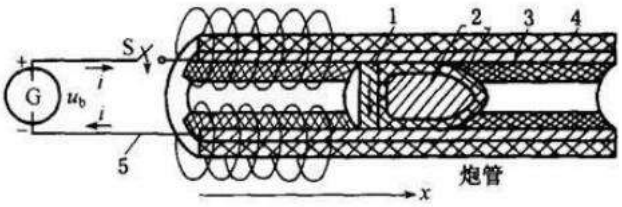

Figure 6. Simulation experiment circuit diagram

5.2 Parameter Measurement

5.2.1 Actual Distance Value

When the supply voltage is 24.84V, the relationship between the transmission distance and the PWM is:

$$Y = -0.0101X^2 + 2.1057X + 3401 \quad (12)$$

Calculate the PWM value according to the formula, input the d value with different distance from the matrix keyboard, and the electromagnetic cannon launches the projectile to different positions of the target. Then actually measure the distance value and calculate the distance error at the same time, as shown in the following table:

Table 4. Measured distance

Distance standard value (cm)	PWM calculation	Distance actual value (cm)	Distance error
210	3398	210	0
230	3351	231	0.0043
255	3281	256	0.0039
270	3233	272	0.0074
290	3162	291.5	0.0052

From the table, it can be analyzed that the distance error is small and meets the requirement that the absolute value of the distance deviation is less than 50cm, indicating that the system can complete the basic requirements (2).

5.2.2 Relationship between Angle and PWM

The title requires that the circular target is placed hori-

DOI: https://doi.org/10.26549/met.v4i1.3242

zontally on the ground, and the position of the bull's eye is within the range of an angle a?30 ?from the center axis. For the convenience of calculation, 30 ?left of the central axis is used as the experimental calibration 0 ? and 30 ?right of the central axis is used as the experimental calibration 60 ?

The relationship between angle and PWM is:

$$Y = -0.0032X^2 - 20.81X + 3354.6 \quad (13)$$

Calculate the PWM value according to the formula. Use the keyboard to input the distance d between the center of the ring target and the calibration point and the deviation angle α from the center axis to the electromagnetic gun. The actual measurement results in an angle value, and the angle error is calculated at the same time. The following is the recorded experimental data:

Table 5. Measured angle

Standard value of angle (degrees)	PWM value	Actual angle (degrees)	error
0	3100	2	0.07
10	2950	11	0.1
30	2680	32	0.07
50	2420	49	0.02

From the table, it can be analyzed that the distance error is small, and the measured distance is combined with the actual value. It meets the requirements for automatic aiming and shooting of the electromagnetic gun after one-key startup, indicating that the system can fulfill the basic requirements (3).

5.2.3 Play part

Part of the task is combined with the OpenMV4 camera and the relationship between distance, angle and PWM, which can achieve the positioning of distance and angle.

6. Summary and Perception

The construction of the mechanical structure is very important. The structure is constantly adjusted and the chip is replaced. There were many problems in the middle, but they were finally resolved. From writing the code to the final success display and completing the test, I have experienced countless debugging and improvements in the middle. Fail, think, discuss, adapt, test, and solve the unexpected difficulties you face again and again. It is also a challenge for us, but persistence is our unanimous belief. Now that you can choose a challenge, you must do it with all your heart. At the same time, communicate with your own team members and other team members. This will not only promote the learning of our team members, but also find and deal with problems in time.

References

[1] Liu Huoliang and Yang Sen, STM32 Library Development Practical Guide, Beijing: Machinery Industry Press, 2008.

[2] Tan Haoqiang. C language programming [M]. Beijing: Tsinghua University Press, 2012.

[3] Huang Ying. Two self-made controllable electromagnetic gun models are used to demonstrate the law of electromagnetic induction in university physics. [D]. Journal of Central China Normal University (Natural Science Edition). 2012. (01): 89-91.

[4] Hu Dezhi, Li Haijun, Wang Yuxin, et al. Design and production of three-stage coaxial coil electromagnetic gun model [D] .Journal of North China Institute of Science and Technology, 2010,7 (1): 85 -87.

 DOI: https://doi.org/10.26549/met.v4i1.3242

SYNERGY PUBLISHING PTE. LTD.

Modern Electronic Technology

https://ojs.s-p.sg/index.php/met

ARTICLE

Analysis of Drone Fleet Type and Quantity for Medical Package Distribution in Emergency System

Yujie Jiang[1] Shizhong Ma[2*] Shilong Zhu[3]

1. School of Economics, North China University of Science and Technology, Tangshan, Hebei, 063210, China
2. College of Electrical Engineering, North China University of Science and Technology, Tangshan, Hebei, 063210, China
3. College of Science, North China University of Science and Technology, Tangshan, Hebei, 063210, China

ARTICLE INFO

Article history
Received: 17 January 2020
Revised: 24 January 2020
Accepted: 9 April 2020
Published Online: 16 April 2020

Keywords:
Emergency response system
Multi-objective mixed integer programming
Drone fleet

ABSTRACT

In order to cope with the disasters caused by the worst hurricane in Puerto Rico in 2017, it is necessary to build an emergency system to reduce the losses. An emergency system should include the location of ISO standard dry cargo containers and the distribution of emergency medical packages. This paper discusses the distribution of emergency medical package. Based on the above location results of ISO standard dry cargo container, taking the demand of disaster areas not exceed its supply into consideration and considering the timeliness and weak economy, a multi-objective mixed integer programming model is constructed on the premise of minimum transportation time and cost. It is determined that the drone fleet consists of four B, one C and one F drones. Through the optimization model, the distribution plan of emergency medical packages is formulated.

1. Emergency Medical Package Allocation Model

If a disaster area is supported by multiple reserve points, it is assumed that multiple reserve points support the disaster area on average. The demand of the disaster area is distributed to the reserve point on average, and the formula is as follows: $a_{ij} = \frac{1}{n} b_j$, Among them, a_{ij} represents the demand of the j th disaster area supported by the i th reserve point and b_j represents the total demand of the j th disaster area. The formula for calculating the demand of reserve point is $P_i = \sum_{j=1}^{n} a_{ij}$, where p is the demand of the i th reserve point.

In order to simplify the model, considering that the distribution of emergency medical packages is a dynamic process, hypothetical conditions are proposed.

(1) Transportation time and cost are calculated accurately. There are no accidents on the way, and the cost is only related to the length of transportation.

**Corresponding Author:*
Shizhong Ma,
Corresponding address:East District of North China University of Technology No. 21 Bohai Avenue, Tangshan Bay Ecological City, Caofeidian District, Tangshan City, Hebei Province, China;
E-mail: 1643360071@qq.com

DOI: https://doi.org/10.26549/met.v4i1.3239

(2) The demand of the reserve point can be supplied in the first time without additional production and supply.

According to the above analysis and given parameters, in the process of emergency rescue, due to the timeliness and weak economy, the time and cost of rescue are minimized within the prescribed rescue time. According to the above analysis, the constraints of the model are summarized as follows:

(1) The total number of emergency medical packages dispatched from each reserve point does not exceed its reserve;

(2) The total number of emergency medical packages accepted by a reserve point is equal to its demand.

(3) The time of dispatching emergency medical packages to each reserve point does not exceed the prescribed rescue time.

Based on the above assumptions and analysis, the following models are established:

$$\min T = \max\left\{x_{ij}T_{ij}\right\}$$

$$\min G = \sum_{i=1}^{m}\sum_{j=1}^{n} x_{ij}C_{ij}$$

$$s.t.\ \begin{cases} \sum_{j=1}^{n} x_{ij}G_{ij} \le G_i \\ \sum_{i=1}^{m} x_{ij}G_{ij} = D_j \\ \sum_{j=1}^{n} D_j \le \sum_{i=1}^{m} G_i \\ T \le T_0 \\ x_{ij} = \{0,1\} \end{cases}$$

Among them, m refers to the number of reserve points marked as $A_1, A_2,...,A_m$; x_{ij}: when emergency medical packages are delivered from reserve point A_i to reserve sites B_i, x_{ij}=1 , otherwise x_{ij}=0.

2. The Solution of Drone Fleet and Emergency Medical Packages Distribution Model

Firstly, the flight speed and duration of drone are taken as the index to evaluate its performance. The performance of drone is ranked as B, F, C, G, D, E, A and H. Due to the limited load capacity and warehouse capacity of drone, we can get how many medical packages each drone can carry:

Table 1. Quantitative analysis table of medical package carrying capacity of drone

Drones' type	A	B	C	D	E	F	G	H
MED1	1	2	4	1	2	2	2	N
MED2	1	2	5	1	3	3	3	N
MED3	1	2	3	1	2	2	2	N

Then the problem of emergency medical package allocation is solved. When solving the problem of medical package allocation, it is assumed that the transportation cost is only proportional to the distance between routes. Therefore, the model is simplified to:

$$f_{\min} = \sum_{i=1}^{m}\sum_{j=1}^{n} x_{ij}T_{ij}$$

$$s.t.\ \begin{cases} \sum_{j=1}^{n} x_{ij}G_{ij} \le G_i \\ \sum_{i=1}^{m} x_{ij}G_{ij} = D_j \\ \sum_{j=1}^{n} D_j \le \sum_{i=1}^{m} G_i \\ x_{ij} = \{0,1\} \end{cases}$$

Through calculation, the number of emergency medical packages transported to hospitals is as follows. The daily needs of hospitals in disaster areas for various types of medical packages are 7 MED1 medical packages, 2 MED2 medical packages and 4 MED1 medical packages. By analyzing the relative distance and the carrying capacity of drone, the optimal drone fleet composition (Table 3) and ISO cargo container packaging configuration (Table 4) are obtained.

Table 2. Optimal fleet composition table for drones

Types and quantities of medical packages	Types and Quantities of Unmanned Aerial Vehicles	Composition of drone fleet
MED1 7	Two B-type and C-type are required respectively.	4 B-types 1 C-types 1 F-type drone
MED2 2	Require a B-Type drone	
MED1 4	Need 1 B-type And F-type drone	

Table 3. ISO Container Packaging Configuration Table

	ISO1	ISO2	ISO3
MED1	6	6	6
MED2	1	1	1
MED3	6	6	6

DOI: https://doi.org/10.26549/met.v4i1.3239

The drone flight plan:According to the analysis and solution of A and B, we make the delivery route of drones as shown in Figure 1.

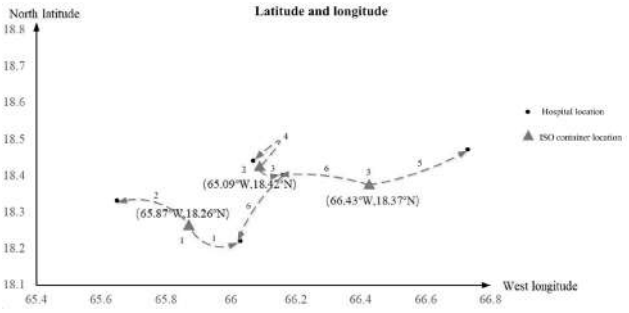

Figure 1. Medical packages delivery route of drones

Generally, there is only one route to the designated medical sites, that is, Route 1 is from container 1 to Caribbean Medical Center, Route 2 is from container 1 to Hospital HIMA, route 3 is from container 2 to Hospital Pavia Santurce, Route 4 is from container 2 to Puerto Rico Children's Hospital, Route 5 is from container 3 to Hospital Pavia Arecibo.

Considering the occurrence of accidents, we set up two more routes, which is from container 3 to Hospital HIMA and Peuerto Rico Children's Hospital. Usually, these two routes are used by drones to detect roads separately, but they can be temporarily used as transportation routes when necessary.

After the analysis and solution of problems A and B, in order to ensure that medical packages can be delivered first every day and the specific road conditions can be known within one day, the following drone delivery schedule is roughly made:

Table 4. The delivery schedule of drone fleet

route	drone type	delivery time	return time
1	B_1	6:00am-6:30am	7:00am-7:17am
2	B_2	6:00am-6:30am	7:00am-7:17am
3	B_3	6:00am-6:10am	6:30am-6:35am
4	B_3+F	7:00am-7:10am	7:30am-7:35am
5	C	6:00am-6:35am	7:00am-7:27am
6(highway investigation)	B_4	6:00am--/14:00pm--/20:00pm--	

Where, drone B_1, drone B_2, drone B_3, and drone F are delivery drones and drone B_4 are reconnaissance drones.

Through the above analysis, our team's packing arrangements for drones are as follows:

Table 5. Packaging arrangement of drone

	B_1	B_2	B_3	F	C	B_4
MED1	1	2	1	1	1	0
MED2	0	0	1	0	0	0
MED3	1	1	0	2	0	0

Delivery drones transport medical packages from reserve sites to the demand sites through strict routes. At the same time, each group of drones transport video configuration, can carry out video recording in the process of cargo transport, provide the company with video basis, combined with independent survey of drone video, so that the company knows the damage or usability of roads, and then on land. Route planning to achieve land rescue.

Starting from the last container, the reconnaissance drones reconnoitre the roads near five demand sites and videotape them to provide timely feedback on road information-damage or usability, so as to facilitate HELP, Inc. to understand the road damage situation, and to provide land rescue to the affected areas, plan rescue time, dispatch rescue personnel and send support equipment. The other drones of types B, except for the first delivery time, reconnoitre the roads around the hospital in the same time as B_4, and report the damage or usability of the roads in time. Since the disaster is sustained, we plan to conduct road reconnaissance three times one day to avoid sudden road damage, which prevent land support from reaching in time.

The specific flight plan is shown in the following figure.

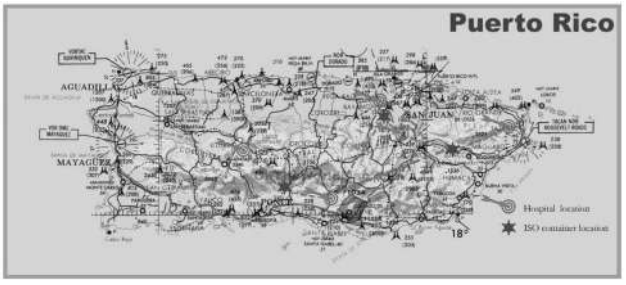

Figure 2. The flight road map of drone Fleet

Reference

[1] Khan J U, Qureshi B A, Zubair S M. A comprehensive design and performance evaluation study of counter flow wet cooling towers[J]. International Journal of Refrigeration, 2004, 27(8): 914-923.

[2] Espadas J, Molina A, Guillermo Jiménez, et al. A

DOI: https://doi.org/10.26549/met.v4i1.3239

tenant-based resource allocation model for scaling Software-as-a-Service applications over Cloud computing infrastructures[J]. Future Generation Computer Systems, 2013, 29(1).

[3] Ben-Elia E, Shiftan Y. Which road do I take? A learning-based model of route-choice behavior with real-time information[J]. Transportation Research Part A: Policy and Practice, 2010, 44(4): 0-264.

[4] Shim D H, Chung H, Kim H J, et al. Autonomous Exploration In Unknown Urban Environments For Unmanned Aerial Vehicles[J]. IEEE Robotics & Automation Magazine, 2005, 13(3).

[5] Henriet F, Stéphane Hallegatte, Tabourier L. Firm-network characteristics and economic robustness to?natural disasters[J]. Journal of Economic Dynamics and Control, 2012, 36(1): 150-167.

 DOI: https://doi.org/10.26549/met.v4i1.3239

SYNERGY PUBLISHING PTE. LTD.

Modern Electronic Technology
https://ojs.s-p.sg/index.php/met

ARTICLE

A Method for Measuring LC Resonance Frequency by Impulse Response

Mingwei Xu* **Jiuxin Gong** **Yuechang Shi**

School of Information Engineering, North China University of Science and Technology, Tangshan, Hebei, 063210, China

ARTICLE INFO

Article history
Received: 17 January 2020
Revised: 24 January 2020
Accepted: 9 April 2020
Published Online: 16 April 2020

Keywords:
LC circuit
Resonant frequency
Digital Storage Oscilloscope
Impulse signal

ABSTRACT

LC circuit resonance frequency measurement often requires the use of professional analysis instruments such as LCR meters, vector network analyzers, but currently such instruments on the market are expensive, and it is difficult for non-professional institute personnel to access. Here comes unnecessary trouble. In view of this situation, a test method for measuring the resonance frequency using only a digital storage oscilloscope is proposed. Using the impulse signal to obtain the system response, the response waveform period can be observed through the oscilloscope.

1. Measurement Principle

This system provides an instantaneous impulse current to the excitation coil to generate a large instantaneous magnetic field. According to the law of electromagnetic induction, the LC circuit under test placed inside the excitation coil will induce an initial impulse current. This initial energy Under-damped oscillation will be generated in the LC circuit. The resonance frequency of this LC circuit can be analyzed by grabbing a piece of oscillation waveform through a digital storage oscilloscope. It is easy to use and has low dependence on high-end instruments. The disadvantage is that the accuracy is limited and it basically depends on the oscilloscope Frequency resolution.

2. Test System Composition

The test system shown in figure 1 is mainly composed of an excitation coil, an impulse current generator, an LC circuit to be tested and a digital storage oscilloscope.

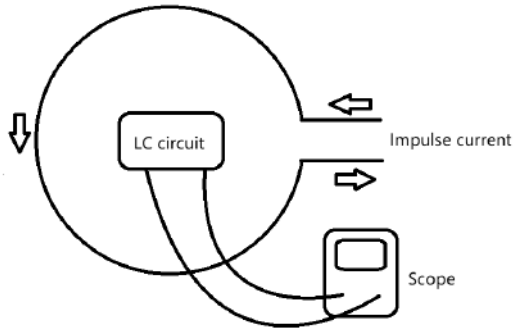

Figure 1. Structure of the test system

2.1 Excitation Coil

The material selection of the excitation coil is based on the internal resistance as a selection criterion. It is better to choose a conductor material that is easy to obtain and has a small internal resistance to allow a large current to pass. In this experiment, a 1.2mm diameter copper enam-

**Corresponding Author:*
Mingwei Xu,
School of Information Engineering, North China University of Science and Technology, Tangshan, Hebei, 063210, China;
E-mail: xumingweiaa@qq.com.

DOI: https://doi.org/10.26549/met.v4i1.3241

eled wire was used to surround the excitation coil.

Since the measurement of the resonance frequency of the LC circuit to be measured is obtained by the voltage waveform generated by its oscillation, and most of the ADCs on the market use 8-bit AD in the internal ADC, the vertical resolution is poor, so the LC circuit the larger the voltage peak generated in the better. Since this system uses the principle of electromagnetic induction to generate an oscillating current in the LC circuit, the larger the voltage generated in the circuit, the greater the magnetic induction intensity generated in the excitation coil. In this experiment, one turn of enameled wire was used to energize the coil.

2.2 Inrush Current Generator

After the number of coil turns is fixed, according to Biot-Savart's law, the magnetic induction intensity generated by the coil is related to the magnitude of the excitation current. The formula is as follows:

$$\vec{B} = \int_L \frac{\mu_0 I}{4\pi} \frac{dl \times \vec{e_r}}{r^2}$$

At the same time, in order to ensure that the excitation current input to the LC system is close to the impulse signal, it is necessary to provide a high-current, short-time narrow pulse signal to approximate the impulse signal. In this experiment, a 10000uF electrolytic capacitor is used to provide instantaneous high current, and a set of relays and MCUs are used to precisely control the charging and discharging of the electrolytic capacitor. The control circuit is shown in figure 2. The relay JK1 controls the charging of the electrolytic capacitor, and the relay JK2 controls the discharge of the electrolytic capacitor. It is necessary to ensure that the two relays cannot be turned on at the same time during charging and discharging, and add a dead time when the state is switched. Failure to do so will cause a short circuit and burn out the relay and excitation coil.

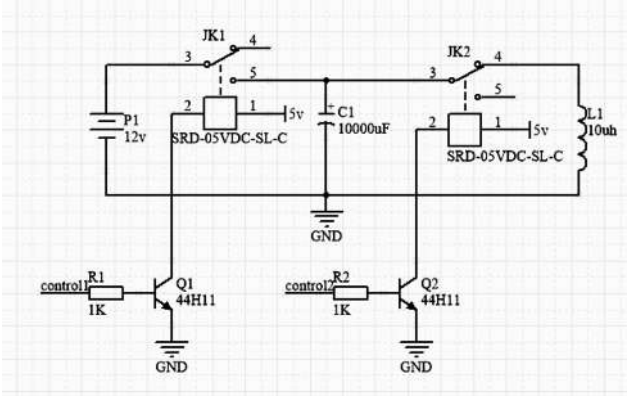

Figure 2. Inrush current control circuit

2.3 LC Circuit under Test

Because this system uses the oscilloscope to capture the voltage waveform of the LC circuit, it is necessary to connect the capacitor and the inductor in parallel to form a series resonance. In this way, you can connect an ordinary oscilloscope probe to both ends of the capacitor or inductor to capture the waveform, as shown in the figure. As shown in figure 3.

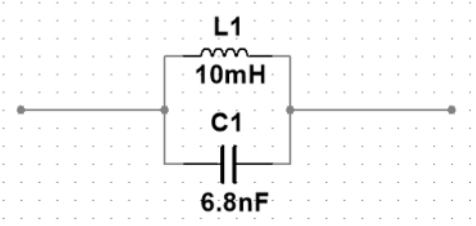

Figure 3. LC circuit

In this experiment, a 10mH I-shaped inductor as shown in figure 4 and a 6.8nF high-frequency capacitor as shown in figure 5 are used to form an LC circuit.

Figure 4. I-shaped inductor

Figure 5. High-frequency capacitor

3. Measurement Steps

3.1 Step 1

Connect the excitation system and check it correctly. Place

 DOI: https://doi.org/10.26549/met.v4i1.3241

the LC circuit under test in the center of the excitation coil. Because the direction of the magnetic induction lines generated in the excitation coil is perpendicular to the horizontal plane where the coil is located, in order to maximize the magnetic field energy received by the LC circuit, it is necessary to make these magnetic induction lines pass through the largest number of I-shaped inductors. When the inductor is placed perpendicular to the plane where the excitation coil is located, the magnetic induction line can pass horizontally through the coil inside the I-shaped inductor to maximize the magnetic field energy obtained. If the inductor is mistakenly prevented from being parallel to the plane where the excitation coil is located, the magnetic field energy is basically not obtained, and the oscilloscope will not capture an obvious voltage waveform.

3.2 Step 2

Set the trigger mode of the digital storage oscilloscope to single trigger mode, turn on the cursor mode, and set the cursor to the tracking mode. After the oscilloscope has set the single trigger mode, it needs an initial trigger level to trigger capture. After the trigger, the oscilloscope will capture the waveform for a period of time. This initial trigger level is replaced by the voltage signal in the LC circuit.

3.3 Step 3

Firstly, the MCU controls the capacitor to be charged, and then controls the capacitor to instantaneously discharge the excitation coil to generate an instantaneous impulse current in the coil. At the same time, the oscilloscope will capture a period of oscillation waveform as shown in figure 6. When the oscilloscope is set after the cursor-tracking mode, for the under-damped oscillation waveform obtained after a single trigger, the time difference between two adjacent peaks or troughs is automatically measured, which is the oscillation period, and the resonant frequency of the LC circuit can be obtained by conversion.

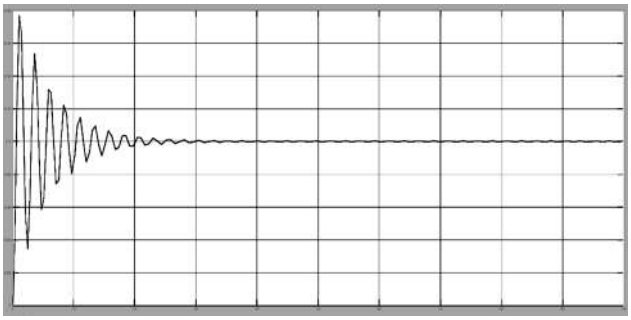

Figure 6. Underdamped Oscillation Waveform

4. Conclusion

Aiming at the method of measuring LC resonance frequency of low-end instruments, this paper proposes a simpler and lower cost measurement method. By setting up a simple test circuit and a low-end digital storage oscilloscope, the LC resonance frequency can be measured more conveniently, but the measurement accuracy often depends on the frequency resolution of the oscilloscope. This also becomes one of the reasons for measurement errors. The result is basically the same as the test result using the LCR tester, and it can be used under limited economic conditions.

References

[1] Resonance characteristics of RLC measured by digital oscilloscope [J]. Li Chaorui. Physical Experiment. 2018 (04)

[2] Li Chaorui.Intuitive measurement method of LC resonance parameters [J] .Physics Experiment, 2019,39 (04): 32-35.

DOI: https://doi.org/10.26549/met.v4i1.3241

SYNERGY PUBLISHING PTE. LTD.

Modern Electronic Technology

https://ojs.s-p.sg/index.php/met

REVIEW

Design and Implementation of Automatic Following Balancing Vehicle Based on UWB Positioning Principle

Chenyu Zhang* **Fangyi Chen** **Zhongyun Kang**

Information Department, Beijing University of Technology, Beijing, 100124, China

ARTICLE INFO

Article history
Received: 27 February 2020
Revised: 5 March 2020
Accepted: 9 April 2020
Published Online: 16 April 2020

Keywords:
Automatic following trolley
UWB positioning
TOF ranging principle

ABSTRACT

With the modernization of industrial production, various automatic following technologies have gradually penetrated into people's lives. Among them, the application fields that follow mobile balancing vehicles range from the structured environment of factories to the daily living environment. The purpose of this subject is to be able to use UWB positioning technology to realize that the balanced trolley is an automatic following function, which mainly uses the ranging function in UWB positioning technology, uses the TOF ranging principle and embedded basic knowledge, and changes the positioning algorithm to a following algorithm. The distance between the target object and the person is effectively determined by two tags set on the trolley and a base station in the hand to determine the distance, and the distance information is transmitted through the serial port. By writing an algorithm, the distance information is converted to the driving information of the trolley, and the driving information is sent to the trolley to control the trolley, thereby realizing the task of balancing the trolley to follow the specified target in a simple indoor environment.

1. Introduction

With the development of wireless communication technology, the world of the 21st century will soon enter the era of wireless interconnection from the network era. Emerging wireless network technologies, such as WiFi, WiMax, ZigBee, Adhoc, BlueTooth, and Ultra-Wide Band (UWB), are widely used in all aspects of public life in offices, homes, factories, parks, etc. The application of wireless network-based positioning technology has broader development prospects.[9]

There are many technologies and solutions for obstacle detection sensors for unmanned vehicles. Commonly used communication technologies include infrared, ultrasonic, radio frequency signals, computer binocular stereo vision sensing, etc., but they are not suitable for indoor signal transmission. Infrared is only suitable for short-distance transmission, and is easily interfered by fluorescent lights or lights in the room. Mobile robots relying on ultrasonic or infrared ranging sensors to avoid obstacles have limited detection ranges and insufficient data at detection points, these defects affect the accuracy of obstacle avoidance control of unmanned vehicles; ultrasonic waves are greatly affected by multipath effects and non-line-of-sight

**Corresponding Author:*
Chenyu Zhang,
female, undergraduate of Beijing University of Technology;
Correspondence address: Room 202, Unit 3, Building 4, District 2, Guoling Town, Changping District, Beijing, China;
E-mail: 1648215006@qq.com.

 DOI: https://doi.org/10.26549/met.v4i1.3366

propagation and cannot be used in indoor environments; radio frequency signals are commonly used in outdoor transmission systems, but they have limitations in indoor systems. Monocular vision can only obtain two-dimensional image information of the environment and cannot obtain depth information of environmental obstacles. Binocular vision has disadvantages such as poor real-time performance and complicated calculation.

It can be seen that with the development of wireless network technology and the increasing demand for follow-up services, the automatic follow-up technology must overcome the shortcomings of the existing technology and meet the following conditions: a) High anti-interference ability; b) High accuracy; c) Low production cost; d) Low operating cost; e) High information security; f) Low energy consumption and low transmit power; g) Small transceiver volume.

None of the above technical solutions can fully meet these requirements. UWB is used for auto-following, which can basically meet the above requirements. UWB is a high-speed, low-cost and low-power emerging wireless communication technology. UWB signals are pulse signals with a bandwidth greater than 500 MHz or a ratio of the baseband bandwidth to the trolleyrier frequency greater than 0.2 (UWBWG, 2001), and have a wide frequency band range. It can be seen that UWB focuses on applications in two fields. On the one hand, it is a short-range high-speed data communication that complies with the IEEE802.15.3a standard, that is, wirelessly transmits a large amount of multimedia data without delay, and the rate must reach 100Mbit/s-500Mbit/s; on the other hand, it is low-speed and low-power transmission in accordance with IEEE802.15.4a, which is used for accurate indoor positioning, such as position detection of battlefield soldiers, industrial automation, sensor networks, home / office automation, robot motion tracking, and so on. The characteristics of UWB signals indicate that it has the advantages of low cost, anti-multipath interference, and strong penetrability in communication, so it can be applied to the positioning and tracking of stationary or moving objects and people, and can provide very accurate positioning accuracy.[1,5,7]

Figure 1. Trolley display screen physical diagram

2. UWB Ranging Module

The TOF development board is based on the official original Evaluation board for new PCB upgrade and development. Based on the EVB, the LCD display and redundant interfaces are deleted to optimize power supply design and routing. The module also uses the STM32F105 microcontroller as the main control chip, which inherits and optimizes the official embedded code to the greatest extent. Peripheral circuits include: DWM1000 module (DWSMA module + 40/pcs), power module, LED indicator module, DIP switch, etc. The development board can be used as a base station or a tag, and can be switched by a DIP switch.

2.1 Main Control Chip: STM32 F105

STM32F105 is an interconnected 32-bit ARM-based microcontroller with 64 or 256K bytes of flash memory. It has USB OTG, Ethernet, 10 timers, 2 CAN, 2 ADCs, 14 communication interfaces.[8]

2.2 Communication Chip: DW1000

The DWM1000 module is an ultra-wideband transceiver module designed based on the DW1000 chip of DECAWAVE. This module integrates the antenna and all RF circuits, power management and clock circuits. This module can be used in TWR or TDOA positioning systems to locate targets with an accuracy of less than 10CM; and the module supports data transmission rates up to 6.8MBPS.[12]

2.3 Ranging Algorithm

TOF (Time of Flight): The ranging method is a two-way ranging technology. It mainly uses the time of flight between two asynchronous transceivers (Transceiver) to measure the distance between nodes. In the line-of-sight environment, the TOF-based distance measurement method has a linear relationship with distance, so the results will be more accurate. We record the time between the data packet sent by the sender and the response as TTOT, and the time interval between the time the data packet is received and the response sent by the receiver is TTAT, then the time TTOF of the unidirectional flight of the data packet in the air can be calculated as:

$$TTOF = (TTOT-TTAT) / 2$$

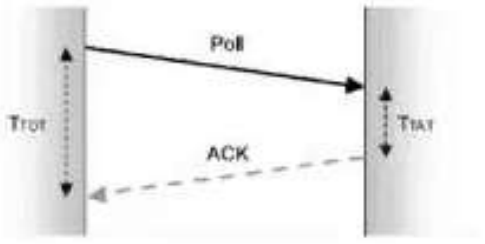

Figure 2. Ranging algorithm schematic diagram

DOI: https://doi.org/10.26549/met.v4i1.3366

But the simple TOF algorithm has a stricter constraint: the sending device and the receiving device must always be synchronized

TW-TOF (two-way time of flight method):

(a) Unilateral two-way ranging

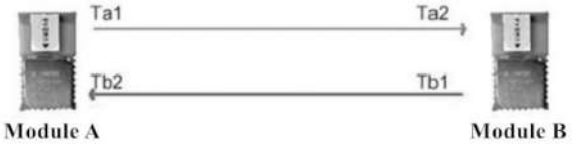

Figure 3. Unilateral two-way ranging algorithm schematic diagram 1

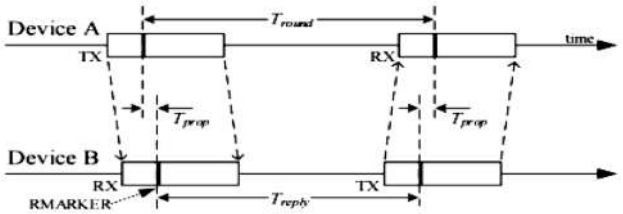

Figure 4. Unilateral two-way ranging algorithm schematic diagram 2

Device A first sends a data packet to device B, and records the time of sending the packet Ta1. After receiving the data packet, device B records the time of receiving the packet Tb1. After that, device B waits for the Treply moment and sends a data packet to device A at the time Tb2 (Tb2 = Tb1 + Treply). After receiving the data packet, device A records the time value Ta2. Then you can calculate the time Tprop of electromagnetic waves in the air, multiplying the time of flight by the speed of light is the distance between the two devices.

Because device A and device B use separate clock sources, the clocks will have a certain deviation. Assuming that the actual frequency of the clocks of device A and device B is eA and eB times the expected frequency, then the error introduced by the clock deviation is: error = Tprop × (1- (ka + kb) / 2).

(b) Bilateral two-way ranging

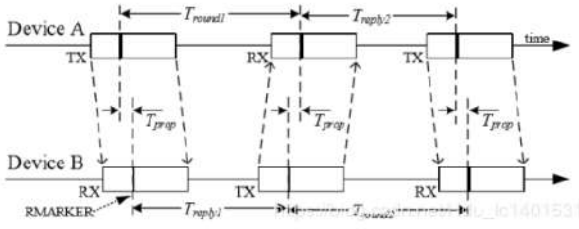

Figure 5. Bilateral two-way ranging algorithm schematic diagram

$$\hat{T}_{prop} = \frac{(T_{round1} \times T_{round2} - T_{reply1} \times T_{reply2})}{(T_{round1} + T_{round2} + T_{reply1} + T_{reply2})}$$

DS ranging is based on SS ranging, and one more communication is added. The two communication times can compensate each other for errors introduced by clock skew.

The error introduced by the DS ranging method clock is: error = Tprop × (1- (ka + kb) / 2).

Suppose the clock accuracy of device A and device B is 20ppm (very poor), and 1ppm is one millionth. Then Ka and Kb are 0.99998 or 1.00002 respectively, and ka and kb are the ratios of the actual frequency and the expected frequency of the clocks of the devices A and B, respectively. The distance between equipment A and B is 100m, and the flight time of electromagnetic waves is 333ns. Then the error introduced by the clock is 20 * 333 * 10-9 seconds, the ranging error is 2.2mm, which can be ignored.[4]

3. Trolley Hardware Module

3.1 Main Control Module

The STM32F103xC, STM32F103xD and STM32F103xE enhanced series use the high-performance ARM® Cortex ™ -M3 32-bit RISC core and operate at 72MHz, built-in high-speed memory (up to 512K bytes of flash and 64K bytes of SRAM), rich enhanced I / O ports and peripherals connected to two APB buses. All devices include three 12-bit ADCs, four general-purpose 16-bit timers, and two PWM timers. They also include standard and advanced communication interfaces: up to 2 I2C interfaces, 3 SPI interfaces, 2 I2S interfaces, 1 SDIO interface, 5 USART interfaces, a USB interface and a CAN interface. The STM32F103xx high-capacity enhanced series operates in the temperature range of -40 ° C to + 105 ° C, and the power supply voltage is 2.0V to 3.6V. A series of power saving modes guarantee the requirements of low power consumption applications. STM32F103xx high-capacity enhanced series products provide 6 different package forms from 64 pins to 144 pins; the configuration of the peripherals in the device varies depending on the package. Below is a basic introduction to all the peripherals in this series of products.[11]

3.2 Motor Drive Module

TB6612FNG is a driver chip for DC motors, whose output transistor uses a low-resistance LD-MOS structure. The two input signals IN1 and IN2 can select one of four modes, such as CW, CCW, short brake and stop modes.[10]

 DOI: https://doi.org/10.26549/met.v4i1.3366

3.3 Balance Module

MPU6000 (6050) is the world's first integrated 6-axis motion processing component. Compared with the multi-component solution, it eliminates the problem of the difference between the time axis of the combined gyroscope and the accelerator and reduces a lot of packaging space. When connected to a three-axis magnetic timing, the MPU-60X0 provides a full 9-axis motion fusion output to its main I2C or SPI port (SPI is only available on the MPU-6000).[6]

4. System Model and Algorithm

The realization of the auto-following balance trolley based on the UWB positioning principle needs to implement data reception, conversion processing, control of the trolley according to distance information, etc. Take one-to-one communication as an example to build a system model and data processing flow:

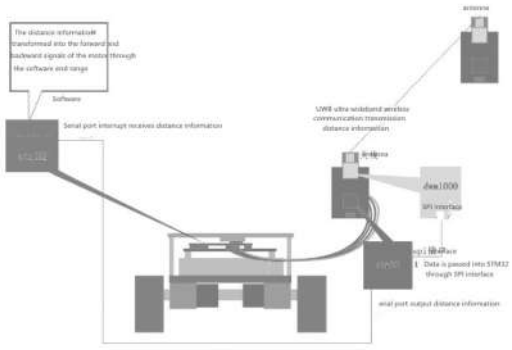

Figure 6. Communication principle between the trolley module and the ranging module

In order to realize the function of turning in the left and right of automatic following, the realization of the automatic following balancing trolley based on the UWB positioning principle requires three positioning modules.

Base station 0 is connected to serial port 2 of the trolley through a serial port, base station 1 is connected to serial port 4 of the trolley through a serial port, and a person holds a tag 0 to send and receive distance information data. The main control chip of the trolley stores two distance information and makes a judgment. First, determine the distance between the two, convert it into a left-turn and right-turn instruction, and then calculate the vertical distance through a mathematical formula. And the distance between the two base stations and the tags are displayed on the OLED screen of the trolley.

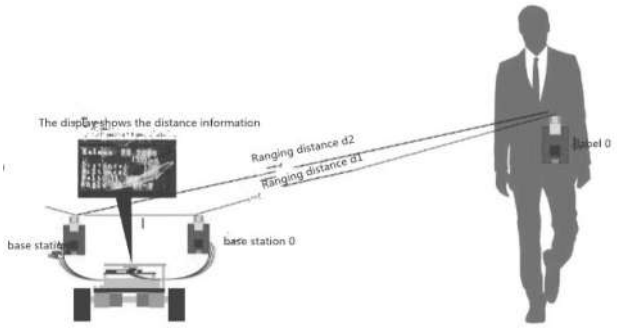

Figure 7. Trolley auto-following Schematic diagram

Vertical distance calculation algorithm:

(a) First compare the sizes of d1 and d2, and perform left and right turn control (until d1> d2: turn right; d1 <d2 turn left).

(b) Calculate the vertical distance through the mathematical formula of the triangle: Knowing the distance L between the base station 1 and the base station 2, the UWB ranging module actually measures the distance between each base station and the tag. The distance between base station 1 and label 0 is d1, and the distance between base station 0 and label 0 is d2.

Using the known three sides in the cosine theorem, first calculate the cosine of C:

$$cosC = (d\_1 \wedge 2 + d\_2 \wedge 2\text{-}L \wedge 2) / (2d\_1\ d\_2)$$

Then find the sine of C:

$$sinC = \sqrt{}\ (1\text{-}\ (\cos C) \wedge 2)$$

From the properties of the triangle sine theorem, the area of the triangle is obtained:

$$S = 0.5 \times d\_2 \times sinC$$

From $0.5 \times L \times d$ is also the area of the triangle, which is obtained from the principle of equal area: $d = S / (0.5 \times sinC)$.

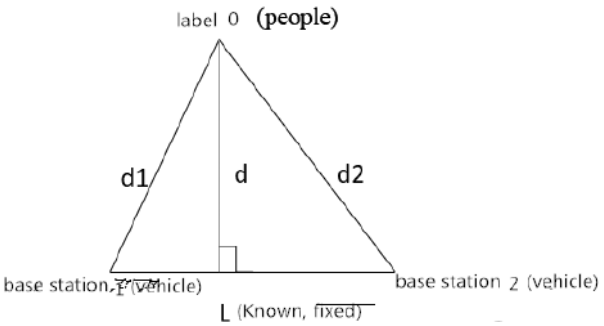

Figure 8. Trolley ranging algorithm schematic diagram

DOI: https://doi.org/10.26549/met.v4i1.3366

The obtained vertical distance can be compared with the set distance. When the vertical distance is less than 1500mm, the trolley is controlled to advance, otherwise the trolley stops.

5. Software Design

After determining the idea through the theoretical model and algorithm, to realize the automatic following of the balance trolley, it is necessary to write the following algorithm as a program. We mainly use mcuisp software to download and update the trolley program through the serial port; use XCOM V2.0 software to test the DW1000 chip, realize serial communication data transmission, modify the transmission distance information format, and display the distance information on XCOM V2.0 serial debugging assistant software.

6. Experimental Tests and Results

The experimental location was set in a house with obstacles, and the ambient temperature was about 20 °C. The final design of the trolley runs smoothly, and the corners are in good driving conditions. When the trolley is driven for a long time, the overall performance of the trolley is relatively stable, with occasional large deviations. As shown in Figure 9, three different follow-up route tests were performed on the trolley. The experimental results are listed in Table 1. In general, the trolley designed in this paper can realize the automatic follow target more accurately and smoothly.[2]

Table 1. Test results of the following routes

Following curve	Number of experiments	Number of Successes	Average time	Success rate
straight line	6	6	35	100%
S-shape (turn over 30 °)	6	6	38	100%
Round	6	5	45	83.3%

Notes: All following lengths are 5000mm and the following vertical distance is 1500mm.[2]

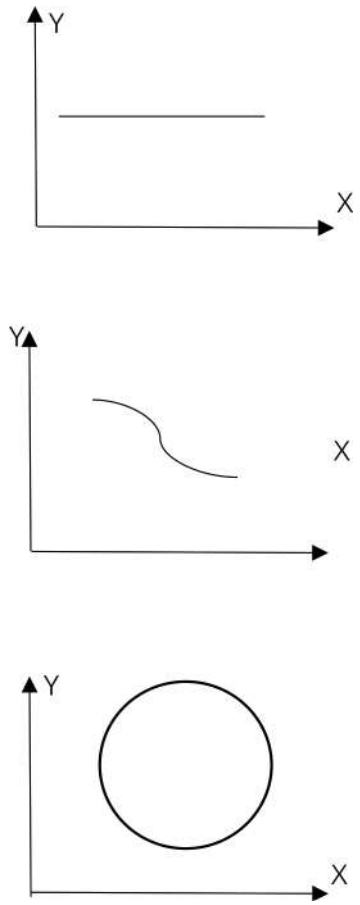

Figure 9. The experimental route schematic diagram

7. Conclusion

This paper designs an automatic following trolley based on the UWB positioning principle, and explains in detail the UWB module ranging principle, the hardware structure of the trolley, and the following algorithm. The trolley is suitable for indoor and outdoor obstacle environments, and can be modified to automatically follow the trunk and the factory automatically follow the small loading truck. There are certain defects in this trolley person. For example, when encountering obstacles such as large partitions, they cannot automatically detect and avoid; the base station cannot make correct judgments about the situation behind the balance trolley itself, and people need further experimental research to improve it.

References

[1] Liang Jiuying. Wireless positioning system[J]. Beijing: Electronic Industry Press, 2013:132-400.

[2] Liu Jinhai, Wang Bofan, Zhou Long, Zheng Yuejiu, etc. Design of automatic following trolley based on UWB technology[D]. Shanghai: University of Shanghai for Science and Technology, 2019.

[3] Fang Chenchen. UWB-based autonomous following robot positioning method[D]. Shanghai: University of Shanghai for Science and Technology, 2016.

[4] Xiongda UWB. Xiongda UWB tutorial series[EB/OL]. 2019-08-25.

[5] Andrew S. Tanenbaum. Computer network[J]. Beijing: Tsinghua University Press, 2012:85-89, 248-

 DOI: https://doi.org/10.26549/met.v4i1.3366

251.
[6] LeeDy.Li. MPU-6000 / MPU-6050 Product description[DB/OL]. 2013-01-07.
[7] Theodore S. Rappaport, Meng Qingming, etc. Principles and Applications of Wireless Communication (Second Edition)[J]. Beijing: Electronic Industry Press, 2018:85-89, 120-122, 256-276.
[8] Liu Huoliang, Yang Sen, etc. Practical Guide for STM32 Library Function Development (Second Edition)[J]. Beijing: Machinery Industry Press, 2017:15-20, 102-205.
[9] Zheng Fei. Application of TDOA-based CHAN algorithm in UWB and NLOS environments[D]. Guilin: University of Electronic Science and Technology of China, 2016.
[10] TOSHIBA. TB6612FNG[DB/OL]. 2012-11-01.
[11] STM32F103xCDE data manual English 5th edition.2009-3.
[12] DECACAVE.DW1000 USER MANUAL.2016.

DOI: https://doi.org/10.26549/met.v4i1.3366

SYNERGY PUBLISHING PTE. LTD.

Modern Electronic Technology

https://ojs.s-p.sg/index.php/met

REVIEW

Time Prediction Through A Congested Road Section

Ziyi Cheng* **Ziqi Wei** **Xinhao Huang** **Ying Li**

Mathematical Modeling Innovation Lab, North China University of Science and Technology, Tangshan, Hebei, 063210, China

ARTICLE INFO

Article history
Received: 8 February 2020
Revised: 15 February 2020
Accepted: 9 April 2020
Published Online: 16 April 2020

Keywords:
Cellular automata
Simulation
BP neural network
Traffic jam

ABSTRACT

First, the cellular automaton was used to simulate a "T" junction, and the correlation analysis was performed by combining the traffic pattern and the corresponding data to obtain the reason for the inaccurate prediction time of the navigation software. The collected data is preprocessed to obtain the driving time of multiple road vehicles in a week, and this is used as the influencing factor. Reuse the collected information: the length of the intersection, the average speed of real-time vehicles at the intersection, and the length of the intersection. The first two processes of the three pre-processing processes are considered together to obtain a time-dependent factor. The correlation factors and the duration of the intersections are used to predict the results of neural network training. Based on the analysis and prediction of the data, the causes of urban traffic congestion are analyzed, and measures to reduce urban congestion are proposed.

1. Introduction

With the acceleration of urbanization and the rapid growth of urban vehicle ownership, traffic congestion is becoming serious. Navigation software mainly considers speed limits and average speed when predicting transit time. However, in the case of traffic congestion, the predicted time differs greatly from the actual time. Therefore, it is of great significance to establish of a traffic congestion prediction model which accurately predicts the time to pass the traffic jam.

2. Determine the Relationship

2.1 Road Traffic Simulation Model

Study the relationship among traffic flow, traffic density, and average vehicle speed.

The relationship between traffic density (p) and traffic flow (N) is:

$$P = \frac{N}{L}$$

**Corresponding Author:*
Ziyi Cheng,
Mathematical Modeling Innovation Lab, North China University of Science and Technology;
Research direction: Accounting;
E-mail: 2697015544@qq.com;
About other authors:
Ziqi Wei, Research direction: Mathematics and Applied Mathematics; E-mail: 1441458258@qq.com;
Xinhao Huang, Research direction: Image Processing; E-mail: 414087068@qq.com
Guidance Teacher: Ying Li; Date of birth: September, 1979; Unit: Mathematical Modeling Innovation Lab, North China University of Science and Technology; Research direction: Data mining.

 DOI: https://doi.org/10.26549/met.v4i1.3249

Where L is the length of each lane in three directions.

The relationship between average speed (v) and vehicle flow (N) is:

$$v = \frac{Sum(v_i)}{N}$$

Where v_i is the speed of each car?

2.2 Cellular Automaton

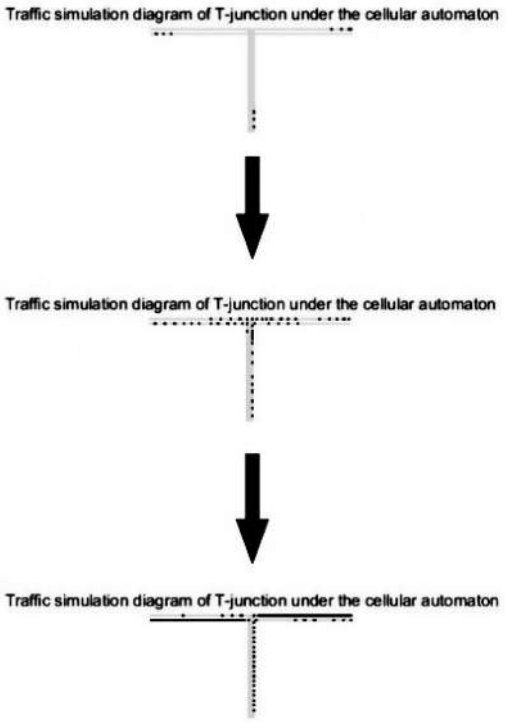

Figure 1. Traffic simulation

As shown in the figure, the road in three directions is regarded as a one-dimensional discrete lattice chain. The simplified vehicle driving rules are: Black cell indicates a car and white cell indicates a car-free. If there is a car in the front square, stop; if there is no car in the front square, move a grid forward.

2.3 Experimental Simulation

2.3.1 Experimental Parameters

Based on the actual situation of the road, visualize roads in MATLAB by defining the matrix. In this experiment, the road length L is 80m. Vehicle speed is a random distribution within 0-2. Vehicles turning at intersections are randomly distributed events. The number of simulation steps is 1000, and the unit step time is 0.01.

2.3.2 Analysis of Results

Some traffic flow, average speed and traffic density data are as follows.

Table 1. Partial data of experimental results

Serial Number	Vehicle Flow(N)	Average Speed($\bar{v}$)	Traffic Density(p)
1	5	0	0
2	5	0	0.0001
...	...	...	...
1000	106	0.6567	0.385

Perform a single factor analysis with considering the impact of traffic density on average vehicle speed. The results are shown in the figure:

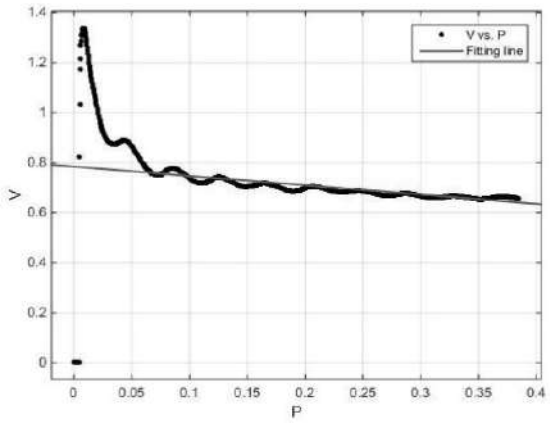

Figure 2. Fit renderings

Correlation coefficient is 0.04831. It can be seen that when the traffic density is 0-0.05, the curve fitting effect is poor and the correlation is not high; when the traffic density is more than 0.05, the curve fitting effect is good and the correlation is high.

So, it is concluded that the vehicle speed is greatly affected by other factors such as subjective factors in the range of 0-0.05. Remove this part of the data, and perform correlation analysis again.

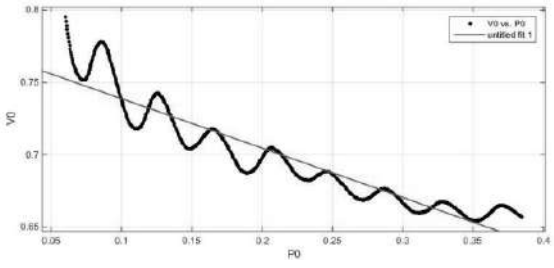

Figure 3. Fitting effect map after 0.05

The correlation coefficient is 0.87 and the correlation is good. It is concluded that when the traffic density is greater than 0.05, the traffic density becomes the main factor

DOI: https://doi.org/10.26549/met.v4i1.3249

affecting the average speed.

Considering the impact of traffic flow and traffic density, perform a two-factor analysis on the intercepted data. The analysis results are as follows:

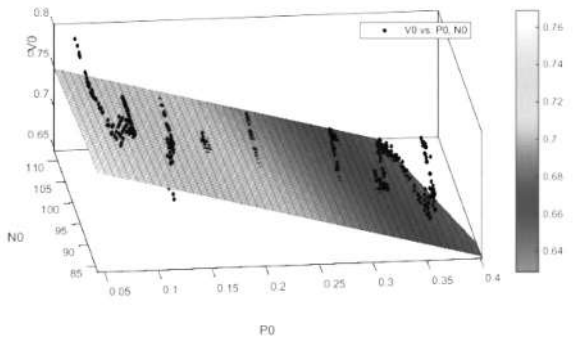

Figure 4. Fitting results of two factor analysis

The correlation coefficient is 0.8921. Therefore, the average speed is affected by traffic flow and traffic density.

3. Time Prediction through Congested a Road Cection

3.1 Establishment of BP Neural Network

Build a BP neural network model with time as the influencing factor. Perform correlation analysis and data image comparison based on 9951391、9981551、9996990、9997010、10355201、10355211、10355221、10387851、10390271、10403841 132456 traffic information flow in a week. The results are as follows:

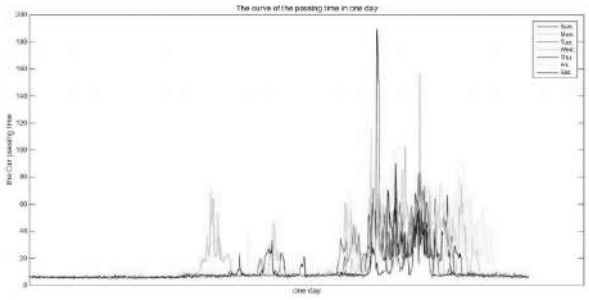

Figure 5. The results

Analysis shows that the rush hour is mainly concentrated in the late rush hour. Road length and average speed are direct factors, while time and week are indirect factors.

3.2 Traffic Time Prediction Model based on BP Neural Network

Preprocess the data used in this article and define the time factor that restricts vehicles from crossing the intersection as: $e_v = \frac{L}{v}$.

3.2.1 Network Construction

The input layer is $X = e_v = [e_{v1}, e_{v2}, ...]$. The output layer is $Y = T = [T_1, T_2, ...]$.

Input layer. The tree of neurons is equal to the number of dimensions of the input vector in the learning sample. Each neuron is a simple distributed hope that passes the input variables directly to the hidden layer.

Hidden layer. The hidden layer output calculation formula is:

$$h(j) = h_j\left(\frac{\sum_{i=1}^{l}\omega_j x_j}{a_j}\right), (j = 1,2,...,l)$$

Output layer. The neuron tree in the output layer is equivalent to the dimension k of the output vector in the learning sample. The output of neuron corresponds to the element of the estimation result. There is a calculation formula:

$$y(k) = \sum_{k=1}^{m}\omega_k h(j), (k = 1,2,...,m)$$

The neural network model has a full-time pruning algorithm. The fine-tuning process is as follows:

$$e = \sum_{k=1}^{m} yn(k) - y(k)$$

Where $yn(k)$ and $y(k)$ are the expected output and the output predicted by the neural network respectively.

3.2.2 Analysis of Prediction Results

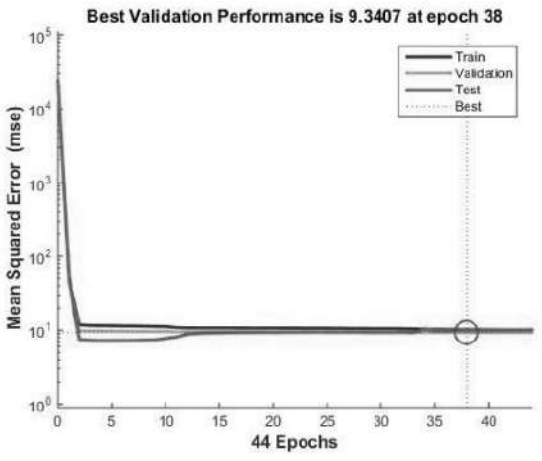

The figure shows that after 44 data iterations, the optimal forecast value of project approval was obtained. The blue line is training data, the green line is validation data, and the red

 DOI: https://doi.org/10.26549/met.v4i1.3249

line is test data. In the above data, 70%: 15:%: 15% training mode is used to obtain the data to be predicted. A functional test of the gradient descent method was performed on the model, and the following results were obtained:

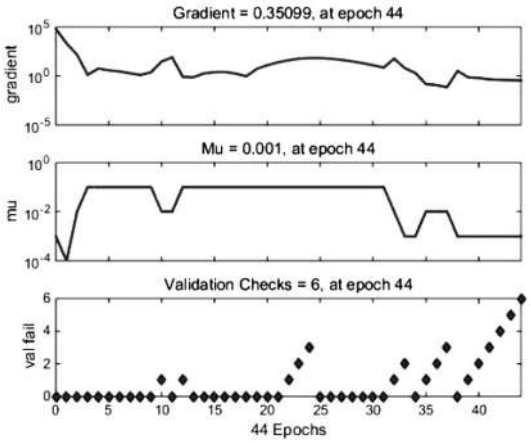

The gradient method is a function of the gradient descent method and has a good effect.

During the validation check training, the system will automatically input the sample data in the validation set to the neural network for validation each time the training is conducted. After inputting the validation set, you will get an error.

If the learning rate is high, the system may be unstable. If the learning rate is low, the training period is too long, and the required error cannot be achieved. In general, we tend to choose a smaller learning rate to keep the system stable and judge by observing the error decline curve.

A rapid decrease indicates that the learning rate is more appropriate, and a larger oscillation indicates that the learning rate is higher. So, due to different network scales, the choice of learning rate must be adjusted.

In order to prevent model training from overfitting, a test analysis was performed on the model. Give the result as follows:

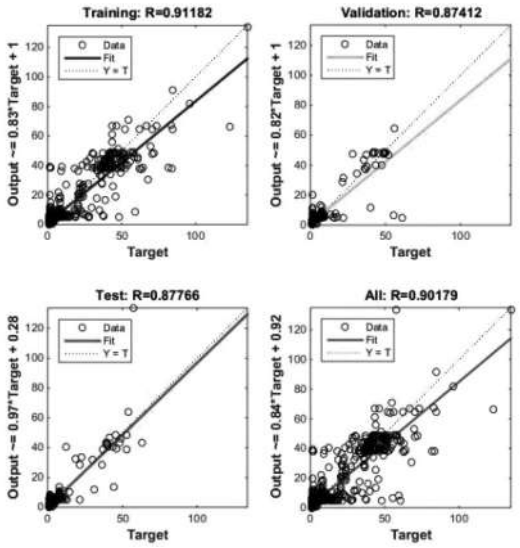

R-squared of training data is 0.91182. R-squared of Validated date is 0.87412. R-squared of Tested data is 0.87766. R-squared for all data is 0.90179. By comparing the training results in this paper, we can see that this model is suitable for real-time road condition prediction.

4. Significance

It is concluded that the predicted time of traffic jam sections is affected by time, week, road length and real-time intersection speed by processing the data of Shenzhen's traffic condition information. In the perspective of big data, the causes of urban traffic congestion are analyzed. On this basis, propose measures for scientific planning to optimize layout and use big data to understand the city. It is of great significance to predict the crux of the traffic congestion problem and new direction of traffic management.

References

[1] Liu Yan. Research on Urban Traffic Operation State Identification and Travel Time Forecasting Method Based on Grid Model [D]. Beijing Jiaotong University, 2018.

[2] Huang Heyaojing, Li Ting. Research on traffic flow state based on cellular automata [J]. Urban Public Transport, 2019 (05): 40-45.

[3] Liu Hang, Song Yingying. Application of queue length model and simulation technology in studying traffic efficiency [J]. Wireless Internet Technology, 2017 (19): 106-107.

[4] Xiong Li, Lu Yue, Yang Shufen. Study on Prediction and Duration of Urban Road Traffic Congestion [J]. Highway, 2017, 62 (11): 125-134.

[5] Zhang Yu. Research on Urban Road Traffic Congestion under the Background of Big Data [J]. Mechanical & Electrical Information, 2019 (29): 162-163.

[6] Deng Jing, Zhang Qian. Traffic flow prediction based on clustering analysis and support vector machine regression [J]. Computer Knowledge and Technology, 2019, 15 (15): 13-16.

[7] Hu Zuoan, Zou Zhengfeng, Bao Tianwen. Traffic information volume prediction method based on BP neural network [J]. Journal of Transportation Engineering and Information Technology, 2018, 16 (04): 81-87.

DOI: https://doi.org/10.26549/met.v4i1.3249

About the Publisher

Synergy Publishing Pte. Ltd. (SP) is an international publisher of online, open access and scholarly peer-reviewed journals covering a wide range of academic disciplines including science, technology, medicine, engineering, education and social science. Reflecting the latest research from a broad sweep of subjects, our content is accessible worldwide – both in print and online.

SP aims to provide an analytics as well as platform for information exchange and discussion that help organizations and professionals in advancing society for the betterment of mankind. SP hopes to be indexed by well-known databases in order to expand its reach to the science community, and eventually grow to be a reputable publisher recognized by scholars and researchers around the world.

SP adopts the Open Journal Systems, see on http://ojs.s-p.sg

Database Inclusion

Asia & Pacific Science Citation Index

Creative Commons

China National Knowledge Infrastructure

Google Scholar

Crossref

MyScienceWork

Tel: +65 65881289
E-mail: contact@s-p.sg
Website: www.s-p.sg